

9. CONSEQUENCES OF EXTREME PHOTON CONFINEMENT IN MICRO-CAVITIES: I. ULTRA-SENSITIVE DETECTION OF PERTURBATIONS BY BIO-MOLECULES

STEPHEN ARNOLD and MAYUMI NOTO
Microparticle Photophysics Laboratory(MP³L)
Polytechnic University, Brooklyn, N.Y. 11201

FRANK VOLLMER
Center for Studies in Physics and Biology,
Rockefeller University, New York, N.Y. 10021

Abstract

It is becoming possible to confine optical photons within a dielectric microparticle (radius~100 μ m) for microseconds. This lifetime would allow a free-ranging photon to travel ~300 m in vacuum. In the frequency domain such a mode resonates with a ratio of frequency to line-width $Q \sim 10^9$. With such a narrow line-width, the sensitivity to size and refractive index perturbations is extreme. An average size change of less than 1 picometer shifts the resonance line through its complete width. These resonances may be stimulated evanescently by coupling to the guided wave in an optical fiber core. Researchers recently used this fiber-microsphere system to detect hybridization of DNA on a microsphere surface, and found that a single nucleotide polymorphism (SNP, one base mismatch) in a long DNA target could be detected with a signal to noise ratio of 54.

1. Introduction

In a previous course at this school in June, 2001 one of us (S. A.) taught about the effect which confinement in spherical micro-cavities has on spontaneous and stimulated emission.¹ Although the experimental photon lifetime within a Photonic Atom Mode (Fig.1, a.k.a. Whispering Gallery Mode) in fused silica was of unprecedented length for an optical microstructure ($\sim 10^9$ oscillations for a $100\mu\text{m}$ radius sphere), it was never as long as theory would have predicted based on a smooth homogeneous dielectric sphere.

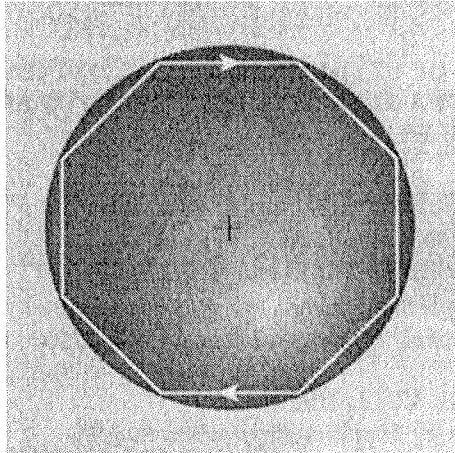


Fig.1 Photonic Atom Mode (a.k.a. Whispering Gallery Mode). Light circumnavigating within a micro-sphere, confined by total internal reflection.

We suspected that the reason was due to sub-nanosopic perturbations associated with molecular roughness. Opportunity is often built on just such problems. Since such resonant micro-cavities might be particularly sensitive to perturbations, why not cause perturbations by attaching nanoscopic particles to the surface, and measure spectral effects caused by them? Biology offers a multitude of uniform nanoscopic particles in the form of protein, DNA, etc. The result of this work was not only to understand the perturbations,^{2,3} but also to generate the world's most sensitive bio-sensor for unlabeled molecules^{4,5}. In what follows we will talk about the perturbation of spherical micro-cavities by presenting theoretical ideas first, and then compare the theoretical results with experiment.

2. Simple Considerations

The picture in Fig.1 easily explains photon confinement, but it takes a wave picture to explain spectral discreteness, and to gain a heuristic awareness of the effects of a geometrical perturbation. Fig.2a takes the wave point of view.

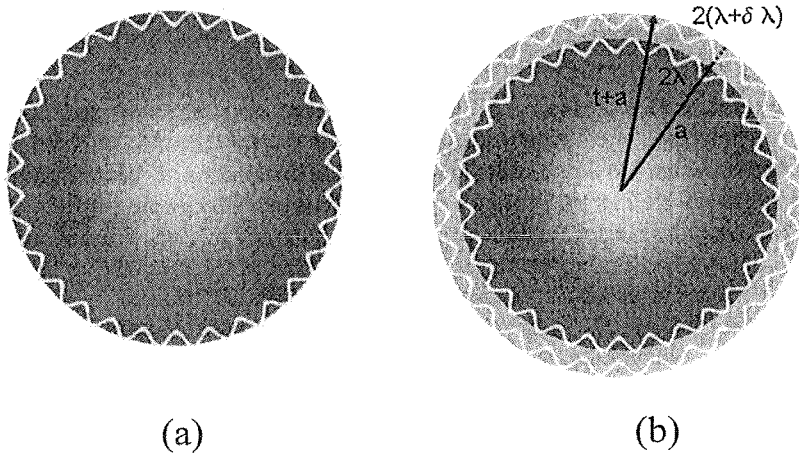


Fig.2 (a) Photonic Atom Mode from a wave point of view; (b) Anticipated wavelength change caused by the addition of a spherically symmetric layer.

One can imagine driving energy into such a mode. To most it should be clear that the only way to drive the mode resonantly is if the wave returns in phase (as shown). In Sec.4 we will outline the means by which this mode can be driven, however at this point we want to characterize our simple mode. There are precisely 30 waves that wrap around the interior circumference in this figure. This will be our mode characteristic or mode number. Suppose now that material of an identical nature and a small thickness t adsorbs on the sphere (Fig.2b). This will cause the wave to circumnavigate a larger circumference, and in order to maintain the same mode number, one might expect the mode wavelength to increase in proportion to the size change. On this basis the fractional increase in wavelength $\Delta\lambda/\lambda$ will be approximately equal to the fractional increase in radius t/a ,

$$\frac{\Delta\lambda}{\lambda} \approx \frac{t}{a}. \quad (1)$$

Suppose now that the adsorbing material is 1 nanometer in thickness. For a sphere having a 100 μm radius, the fractional shift in wavelength according to Eqn.1 would be $\sim 10^{-5}$. This is smaller than the resolution of a grating spectrometer, but is a “piece of cake” (i.e. easy) for the microsphere as a spectrometer. The reason is that the resonances of a microsphere are extremely narrow. Resonances with Q 's of 10^7

(linewidths of 1 part in 10^7) are considered “broad”. But such a “broad” line would shift one hundred times its linewidth for a 1 nm layer. For it to shift just one linewidth requires only a 10 picometer layer (i.e. one tenth the size of a hydrogen atom). So such a small perturbation should be easy to observe.

Our picture thus far is heuristic, and may in fact be incorrect. In Sec. 5 we will see what exact perturbation theory says. However first we will discuss the physical nature of the modes more exactly.

3. Theoretical Approach

As students at this school you likely come from both physical and chemical backgrounds. Extensive theory into electromagnetics is generally not pursued within chemistry departments. However quantum mechanics is common to both. Fortunately an understanding of the electrodynamics of Photonic Atom Modes in a sphere can be gained by reducing the electrodynamic problem to a quantum analog. We will take this approach just as we had in the last school, however here our interest will be to perturb the sphere, and look for particular consequences of this perturbation.

First let us establish the quantum analog. Resonant modes contain photons with quantized angular momentum similar to the electron in a Bohr atom. In order to determine the exact characteristics of these modes one has to solve the Electromagnetic wave equation for a dielectric sphere. In a dielectric microsphere with no excess charge, the governing Helmholtz equation is

$$\nabla^2 \mathbf{E} + k^2 \mathbf{E} = 0. \quad (2)$$

where \mathbf{E} is the electric field, $k = \omega n(r)/c$ is the propagation constant and $n(r)$ is the refractive index. Inspired by the orbiting images displayed in Figs.1 and 2, and the spherical symmetry associated with the problem, we emphasize the importance of the angular momentum by constructing the Laplacian using the angular momentum

operator $\hat{L} = -i(\vec{r} \times \nabla)$; $\nabla^2 = \left(\frac{1}{r} \frac{\partial^2}{\partial r^2} (r) - \frac{\hat{L}^2}{r^2} \right)$. Eqn. 1 becomes

$$\left(\frac{1}{r} \frac{\partial^2(\mathbf{r})}{\partial r^2} - \frac{\hat{L}^2}{r^2} \right) \mathbf{E} + k^2 \mathbf{E} = 0 . \quad (3)$$

Considering that the angular momentum operator commutes with its square (i.e. $[\hat{L}^2, \hat{L}] = 0$), a solution to Eqn 3 can be written down by examination, $\mathbf{E} = \hat{L}\psi$. This is a so-called TE mode. With this form \hat{L} can be factored through, leaving Eqn. 3 in the form

$$\hat{L} \left[\frac{\partial^2(r\psi)}{\partial r^2} - \frac{\hat{L}^2(r\psi)}{r^2} + k^2(r\psi) \right] = 0 . \quad (4)$$

This is a convenient form since it is clear that the vector Helmholtz equation can be satisfied so long as the scalar equation within the brackets in Eqn. 4 is set to zero;

$$\frac{\partial^2(r\psi)}{\partial r^2} - \frac{\hat{L}^2(r\psi)}{r^2} + k^2(r\psi) = 0 . \quad (5a)$$

Eqn. 5a can be re-written in the form of a Schrödinger equation. First we set

$$r \psi(\mathbf{r}) = \psi_r(\mathbf{r}) Y_{\ell,m} \quad (5b)$$

and use $\hat{L}^2 Y_{\ell,m} = \ell(\ell+1) Y_{\ell,m}$, where ℓ is the angular momentum quantum number and $Y_{\ell,m}$ is a Spherical Harmonic function with azimuthal quantum number m . Next we add and subtract $k_0^2 \psi_r$ from the left in Eqn. 5a. With these modifications Eqn. 4a takes the form

$$\frac{d^2 \psi_r}{dr^2} + \{ k_0^2 - [k_0^2(1-n^2) + \ell(\ell+1)/r^2] \} \psi_r = 0 , \quad (6a)$$

which is clearly identified as a Schrödinger-like equation, in which the effective energy is k_0^2 and the effective potential ⁶

$$V_{\text{eff}}(\mathbf{r}; k_0, n, \ell) = k_0^2(1-n^2) + \ell(\ell+1)/r^2 . \quad (6b)$$

This potential is an important key for constructing a perturbation theory, and we will return to it often.

Eqn. 6b describes the behavior of light (trapped photon) inside the dielectric microsphere. The first term in the effective potential is negative and leads to dielectric confinement of light, while the second centripetal term is repulsive. The sum of these two terms generates a potential pocket in which photons can be confined. In Fig 3 we have plotted the effective potential for $\ell = 23$, $n = 1.41$, and $k_0 = 10^5/\text{cm}$, for a sphere with radius, $a = 1.94 \mu\text{m}$.

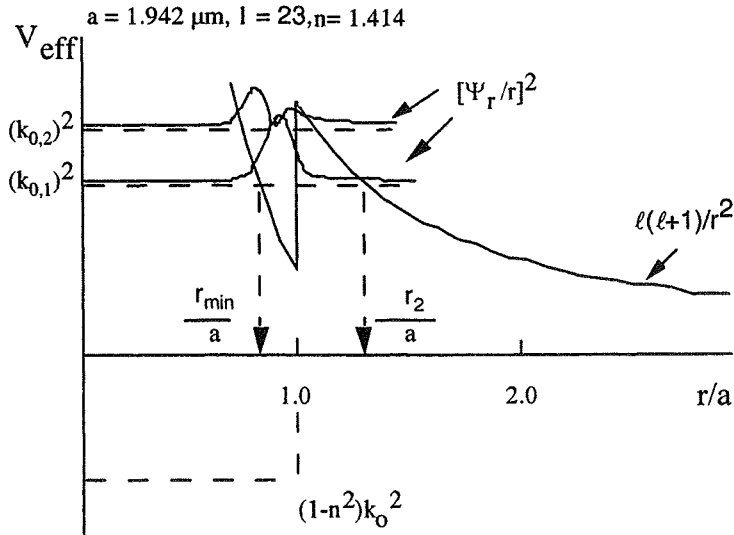


Fig. 3 The effective potential vs. (r/a) for a photonic mode trapped in a dielectric microsphere.

Solutions for ψ^2 at particular values of the effective energy k_0^2 show a substantial buildup of intensity, as seen in Fig.3. These solutions can be stimulated to “resonate” using an external source (i.e. plane wave or evanescent field), and their form conveys a great deal of physical information.

By transforming the independent variable in Eqn 6a from radius r to the product of free space wave vector k_0 times r , we create an convenient “dimensionless length”, which at the surface is known as optical size X ; $X = k_0 a$. For a given refractive index n , the optical size alone identifies the “dimensionless frequency” of a resonance (i.e. as the size changes, the optical size remains constant). If a particle were to grow in size by a small increment δa of identical material, then the free-space frequency of a given resonance must shrink in the same proportion, i.e. $\delta k_0/k_0 = -\delta a/a$, consistent with Eqn.1.

The first two modes plotted above correspond to the lowest order and next higher order resonance with optical sizes, $(k_{0,1} a) = 19.42$ and $(k_{0,2} a) = 23.46$. Note that photons in these states are not strictly confined by “classical turning points”. The photon can extend into “classically forbidden regions” where the effective energy is lower than the effective potential. Most notably, the probability of locating a photon just outside the particle decays exponentially. This is the region of the so-called “evanescent field” which will be described in more detail in Sec. 4. This field is responsible for the interaction with macromolecules just outside the sphere, and is essential for coupling energy into the sphere from a guided wave.

4. Experimental Insights which grow out of the Fig.3

The evanescence demonstrated in each of the resonant solutions in Fig.3 allows us to construct a means for coupling energy into a photonic atom mode of a microsphere. Once again we can learn from quantum mechanics. The electronic wavefunction of a metal decays exponentially just outside at its surface. When two metals are brought close to each other these exponential tails overlap leading to transfer of electrons between the metals due to tunneling. From a photonic standpoint we can affect the same sort of tunneling by overlapping the evanescent tails between confining dielectric structures. A one-dimensional structure for confinement is an optical fiber. If the core of such a fiber is brought close to a microsphere at the correct frequency then the situation illustrated in Fig.4 can occur.

The diminishing amplitude of the guided wave as it passes the microsphere is a consequence of energy loss in the sphere. Actually the system is an interferometer. Tunneling into the fiber is accompanied by a 90° phase shift relative to the wave which proceeds down the fiber. When the light tunnels back into the fiber after many circumnavigations of the microsphere it is subject to an additional 90° phase shift. So the wave arriving back from the fiber at resonance is 180° out of phase with the wave travelling down the fiber. This leads to a spectral dip in the forward going energy (Fig.5).

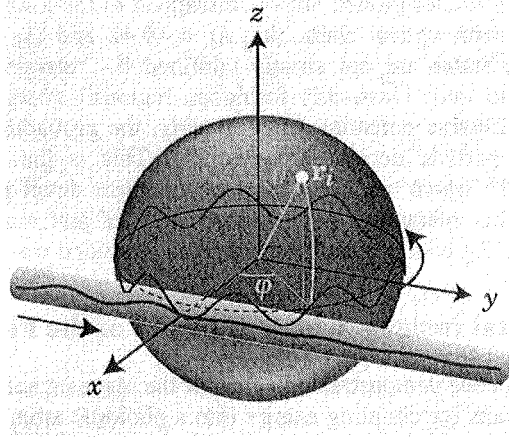


Fig.4 Illustration of coupling of optical energy between a guided wave in an optical fiber and a Photonic Atom mode in a microsphere. The vector r_i points to a small nano-perturbation.

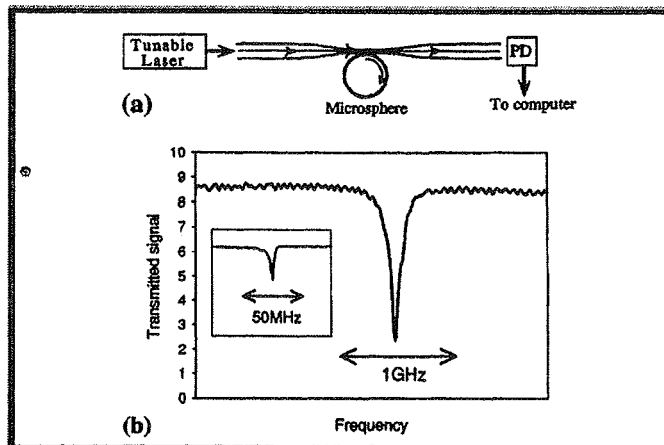


Fig.5 The transmitted light shows a dip corresponding to a Photonic Atom resonance.⁷

A perturbation at the microsphere surface may be expected to lead to a change in the spectral dip (i.e. spectral position or linewidth). The frequency shift of the dip may be expected based on our heuristic model (Eqn.1). This shift will be the basis for transducing the adsorption of bio-molecules. If the surface is conditioned with specific biological recognition elements, the frequency shift can inform us as to the existence of particular bio-molecular interactions (e.g. antibody molecules for antibody-antigen detection, or single stranded DNA for DNA detection through hybridization). Before

presenting experiments, we will estimate the shift from perturbation theory.

5. First Order Perturbation Theory: Spherically Symmetric Layer

Before proceeding we remind the reader of our Quantum analog

$$\frac{d^2\psi_r}{dr^2} + \{k_0^2 - [k_0^2(1-n^2) + \ell(\ell+1)/r^2]\} \psi_r = 0 \quad (6a)$$

This Equation has the usual Schrödinger form, with various analogs listed below;

	Schrödinger	Analog
Energy	E	$E_{\text{eff}} = k_0^2$
Potential	V	$V_{\text{eff}} = k_0^2(1-n^2) + \ell(\ell+1)/r^2$

Table. 1 Quantum Analogs

Adding a nanoscopic layer to the surface leads to a perturbation in the potential,

$$\delta V_{\text{eff}} = \delta[k_0^2(1-n^2)]. \quad (7)$$

This perturbation will lead to a first order energy shift δE_{eff} . The standard result from quantum mechanics is that the first order perturbation in the energy of a quantum level is

$$\delta E_{\text{eff}} = \frac{\langle \psi_r | \delta V_{\text{eff}} | \psi_r \rangle}{\langle \psi_r | \psi_r \rangle}. \quad (8)$$

where V_{eff} is the perturbation of the potential. Using our analogs from Table 1 transforms Eqn.8 to

$$\delta(k_0^2) = \frac{\langle \psi_r | \delta[k_0^2(1 - n^2)] | \psi_r \rangle}{\langle \psi_r | \psi_r \rangle}. \quad (9)$$

The change in the square of the refractive index square is $\delta(n^2) = n_\ell^2 - n_m^2$, where n_ℓ and n_m are the refractive indices of the layer and medium respectively. Furthermore having in mind that the energy k_0^2 will not be constant, we expand Eqn. 9 to;

$$\begin{aligned} \delta(k_0^2) * \langle \psi_r | \psi_r \rangle = & \delta(k_0^2) * \langle \psi_r | \psi_r \rangle + \\ & \langle \psi_r | -k_0^2(n_\ell^2 - n_m^2) | \psi_r \rangle + \langle \psi_r | -2k_0\delta k_0 n_s^2 | \psi_r \rangle, \end{aligned} \quad (10)$$

which reduces to

$$\langle \psi_r | -k_0^2(n_\ell^2 - n_m^2) | \psi_r \rangle + \langle \psi_r | -2k_0\delta k_0 n_s^2 | \psi_r \rangle = 0. \quad (11)$$

Expressing Eqn.11 in terms of integrals;

$$\int_{\text{layer}} -k_0^2(n_\ell^2 - n_m^2) |\psi_r|^2 dv + \int_{\text{all space}} -2k_0 n_s^2 \delta k_0 |\psi_r|^2 dv = 0. \quad (12)$$

With the first integral only taken over a nanoscopic layer on a 100 μm radius sphere, and using continuity for the wave function at the surface

$$\int_{\text{layer}} -k_0^2(n_\ell^2 - n_m^2) |\psi_r|^2 dv \cong -k_0^2(n_\ell^2 - n_m^2) |\psi_r(a)|^2 4\pi a^2 t. \quad (13)$$

In addition with 94% of the square of the wavefunction within the sphere,⁸ the second integral can be reasonably taken over just the interior volume.

$$\int_{\text{all space}} -dv |\psi_r(r)|^2 (2k_0)\delta k_0 n_s^2 \cong \int_0^a -dr 4\pi r^2 |\psi_r(r)|^2 (2k_0)\delta k_0 n_s^2. \quad (14)$$

Therefore according to Eqn. 12, 13 and 14, the fractional shift in frequency $(\frac{\delta\omega}{\omega} = \frac{\delta k_0}{k_0})$, will be

$$\frac{\delta\omega}{\omega} = \frac{\delta k_0}{k_0} = - \frac{a^2 t |\psi_r(a)|^2 (n_\ell^2 - n_m^2)}{2 n_s^2 \int dr r^2 |\psi_r(r)|^2} \quad (15)$$

The volume integral in the denominator of Eqn.15 can be related to the surface value of the square of the spherical Bessel function in the limit in which the wavelength is much smaller than the microsphere radius,⁹

$$\int_0^a j_\ell^2(\sqrt{\epsilon_{rs}} k_0 r) r^2 dr \approx \frac{a^3}{2} j_\ell^2(\sqrt{\epsilon_{rs}} k_0 a) \frac{\epsilon_{rs} - \epsilon_{rm}}{\epsilon_{rs}} \quad (16)$$

Substituting Eqn.16 in the denominator of Eqn.15 gives a differential shift due to accretion of a layer on the surface, where ϵ_{rm} is the relative permittivity of the surrounding medium (e.g. water).

$$-\frac{\delta\omega}{\omega} = \frac{\delta\lambda}{\lambda} = \frac{(\epsilon_{r\ell} - \epsilon_{rm}) t}{(\epsilon_{rs} - \epsilon_{rm}) a} = \frac{(n_\ell^2 - n_m^2) t}{(n_s^2 - n_m^2) a} \quad (17)$$

In Eqn.17 we have presented the 1st order shift in terms of refractive indices and relative permittivities (i.e. $n^2 = \epsilon_r$). Eqn.17 agrees with Eqn.1 when $n_\ell = n_s$, as anticipated heuristically, and is consistent with the shift obtained through detailed electromagnetic theory for a layer on a microparticle in vacuum.¹⁰

One can think of the perturbation problem in terms of molecular properties by imagining the layer to be carved up into a jigsaw pattern. Of course there are few identical shapes that could fit into such a pattern (in a monolayer) without leaving voids. However we will assume that the molecular layer is voidless and return to the question of voids in discussing experimental results in a later section. We will call this model the Voidless Tile Model. It turns out that Eqn.17 is easily transformed by introducing two new parameters: the tile excess polarizability α_{ex} (excluding depolarization effects), and the surface density of tiles σ . By using the constitutive equation $\epsilon\mathbf{E} = \epsilon_0\mathbf{E} + \mathbf{P}$, and applying it to two situations: tile present and tile absent, we arrive at the following expression for the permittivity difference times thickness in the numerator of Eqn.17,

$$(\epsilon_{r\ell} - \epsilon_{rm}) t = \frac{P_\ell - P_w}{\epsilon_0 E} t = \frac{P_{ex}}{\epsilon_0 E} t = \frac{p_{ex} t}{\epsilon_0 E v_t} = \frac{p_{ex} \sigma}{\epsilon_0 E} = \frac{\alpha_{ex} \sigma}{\epsilon_0} \quad (18)$$

where p_{ex} is the excess dipole moment for a tile, and v_t is the tile volume. Using the expression at furthest right in Eqn.18 we obtain

$$\frac{\delta\lambda}{\lambda} = \frac{\alpha_{ex} \sigma}{\epsilon_0(n_s^2 - n_m^2)a} \quad (19)$$

This equation is perfectly correct for a voidless layer which is considerably thinner than the evanescent field depth. However, it is approximately true also for a dilute layer so long as it is uniformly distributed and one can neglect local field effects (i.e. depolarization effects which are always present for partially isolated nanoparticles). It turns out that it is a good approximation for a dilute layer of particles considerably smaller in size than the microsphere (< 50 nm on a microsphere $100\mu\text{m}$ in radius). Under these circumstances the shift will be proportional to the surface concentration as indicated.

Finally we are interested in the possibility for single protein detection. Single protein detection would be possible by looking at steps in the change of $\delta\lambda/\lambda$ with time, and this in turn provides a possible means for separately measuring α_{ex} . Since the light within a WGM circumnavigates the equator ($\theta = \pi/2$) in an orbit which is confined to a thin ring, molecules at polar angles outside the ring cannot influence the mode frequency. The greatest signal comes from molecules which stick at $\theta = \pi/2$. For a TE mode which circulates at the equator $\ell = m$, and the angular intensity is proportional to $|\widehat{L}Y_{\ell\ell}|^2$, which for large ℓ is proportional to $|Y_{\ell\ell}|^2$.¹¹ So the ratio of the frequency shift for a protein at the equator to that averaged over random positions on the surface is enhanced by a factor $EF = 4\pi|Y_{\ell\ell}(\pi/2, \varphi)|^2$. This spatial enhancement EF can be significant. For the average size microparticle anticipated ($a \sim 100\mu\text{m}$), $\ell \sim 1000$ and $EF \cong 36$. To obtain the average shift for an individual protein at a random position, we set the surface density in Eqn. 19 to $\sigma = 1/(4\pi R^2)$ with the result $(\delta\lambda/\lambda)_r = \alpha_{ex} / [4\pi\epsilon_0(n_s^2 - n_m^2)R^3]$. The shift due to a single protein at the equator is $(\delta\lambda/\lambda)_e = EF \times (\delta\lambda/\lambda)_r$, or

$$(\delta\lambda/\lambda)_e = \frac{\alpha_{ex} |Y_{\ell\ell}(\pi/2, \varphi)|^2}{\epsilon_0(n_s^2 - n_m^2)a^3} \quad (20)$$

The first test of all of this theory requires attaching biological nanoparticles to the microsphere and tracking dips in resonances.

6. Experimental Setup

To carry out our perturbation experiments it is necessary to construct a situation similar to the concept in Figs.4 and 5. This requires forming a microsphere and an eroded optical fiber, and touching one against the other while measuring the excitation spectrum of the transmitted light through the fiber. The entire system will be immersed in a buffer solution ($\text{pH} = 7.4$) where protein molecules can fold into their natural biological shape. In what follows we will briefly describe the microsphere and fiber fabrication, the sample cell, and our means for taking high resolution spectra of the microsphere.

To fabricate a microsphere one can simply cut a small portion of the single mode fiber (about 10 cm) and then melt the stripped end of the fiber by exposing it to the butane/nitrous oxide microtorch flame (Microflame, Inc.), while rotating the fiber. As the fiber rotates the melting silica will form into a spheroidal shape under the force of surface tension. A spheroid manufactured in this form can have a radius as small as 70 μm . Such a microspheroid is shown in Fig.6b. The excitation fiber is led from the laser source to the detector and held in place while a 1 cm section is eroded using 25% HF acid. The erosion is terminated when this local portion of the fiber reaches 4 μm in diameter. The fiber can be seen in Fig.6b as what appears to be a narrow vertical line in contact with the microspheroid.

The sample cell shown in Fig.6a is used to contain 1 mL of aqueous buffer solution between the two glass slides (top and bottom) by means of surface tension. It is assembled around the etched portion of the fiber. Two silicone rubbers are placed on each side of the lower glass slide, and the stem of a surface modified microsphere (note: the preparation of the surface will be described) is held between silicone strips on the right side as illustrated in Fig.6a. The opposite side of the cell holds a thermocouple in the same fashion.

The light source has stringent requirements. It must operate at a single frequency with a linewidth smaller than that of a microsphere resonance, and it must be tunable. At first these requirements may seem simple enough until one looks at the specifics. The linewidths of the resonances which are to be interrogated may be as small as 0.00001nm, hardly a width that can resolve with a source consisting of an arc lamp followed by a grating monochromator. For such a source a linewidth below 0.01nm would be challenging to produce. Fortunately the telecommunication community has produced small semiconductor lasers with linewidths in line with our needs.¹² However simple heterojunction lasers cannot be tuned without mode hopping, which is unacceptable. To remedy this situation a Bragg grating is imprinted within the laser and resulting device is

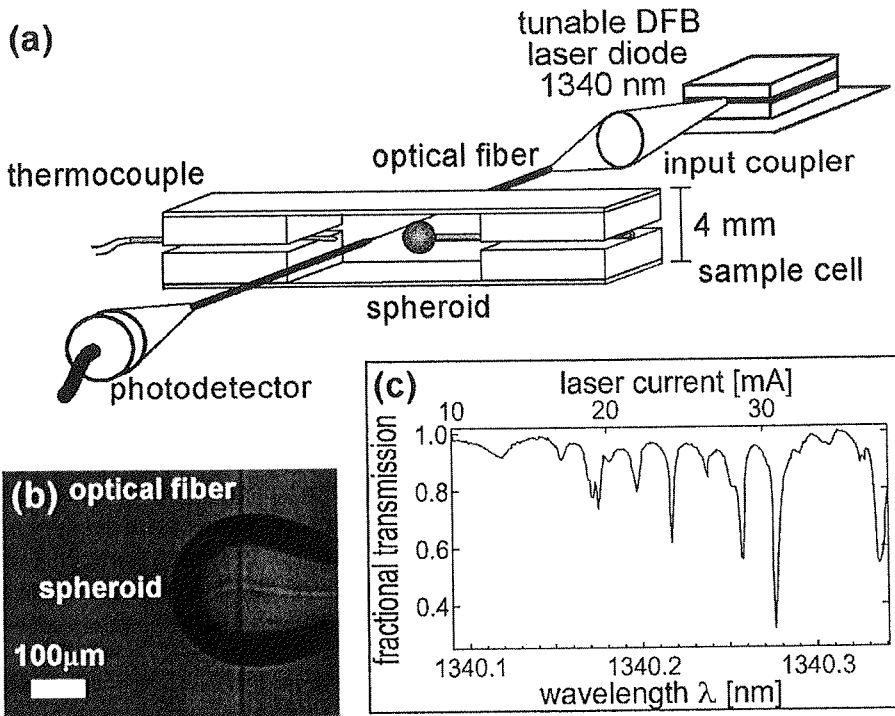


Fig.6 (a) Experimental setup. Optical resonances of a spheroidal glass microparticle are excited by coupling the spheroid evanescently to an eroded single mode optical fiber. (b) Picture of the spheroid coupled to the eroded part of the optical fiber. (c) Resonances dips vs. wavelength.

termed a Distributed Feedback Laser (DFB). The DFB can be easily tuned by changing the drive current or the temperature. For our purposes the temperature was held constant in order to avoid time delays in tuning. The current tuning coefficient, which is $\sim 0.01 \text{ nm/mA}$ is sufficient to locate a resonance in a slightly spheroidal glass microstructures with a radius of a couple of hundred micrometers. Since our research is highly dependent on precise knowledge of the tuning coefficient, measurements independent from the specifications provided by the manufacturer were needed. These measurements were obtained using a scanning Michelson Interferometer.

Fig. 6c shows a typical spectrum of the microsphere while immersed in the buffer solution. Note that the entire sweep of the laser is only $\sim 0.2 \text{ nm}$, but the resonance lines are considerably narrower ($Q \sim 10^6$). Also note that one of the dips in transmission subtracts 70% from the incident light.

7. Experimental Results

To test our perturbation theory we have chosen to use protein molecules. Typically they are a few nanometers in size. An example of an abundantly available protein is Human Serum Albumin (HSA). In fact, it is the most abundant protein in our blood. The bovine form of the protein (BSA) is available in high purity, and has a known crystal structure¹³. The surface of our microsphere must be treated in order to make the protein “stick”.

In our buffer solution BSA carries a negative charge. To promote adsorption to the microsphere the sphere’s surface is modified so as to give it a positive charge. To give the microsphere surface a positive charge it is treated with a solution 3-aminopropyltrimethoxysilane. This compound reacts with the surface and self assembles a “rug” of amine groups (NH_2 , Fig. 7).

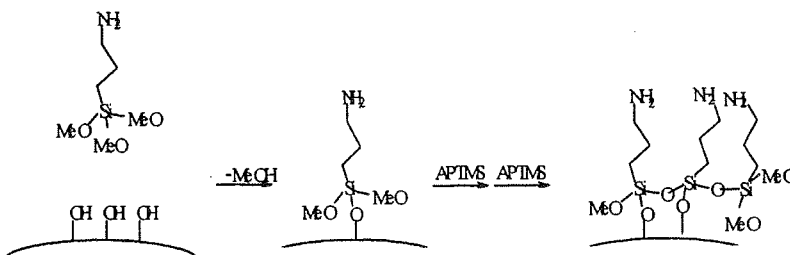
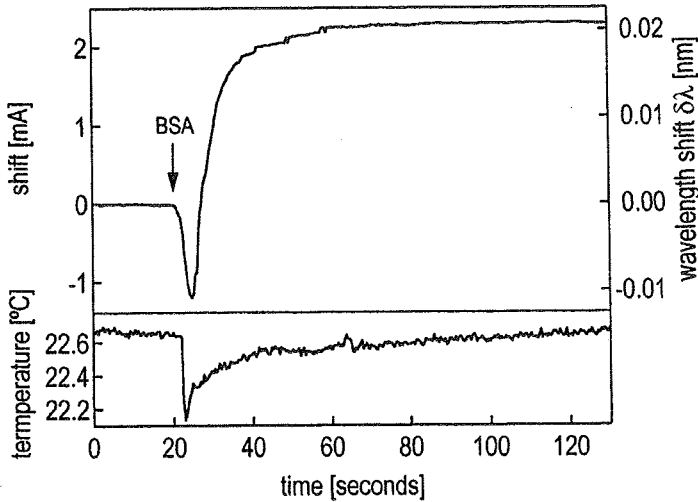


Fig. 7 Chemical action of the silane coupling agent.

The amine groups acquire a positive charge in the buffer solution. So BSA sticks readily to this amine “rug”.

BSA is added to the sample cell by injecting a 10 μL of a BSA buffer solution into the sample cell. The expectation for our first experiment was an increase in the wavelength of a resonance. Fig.8a shows that the effect initially went in the opposite direction.

(a)



(b)

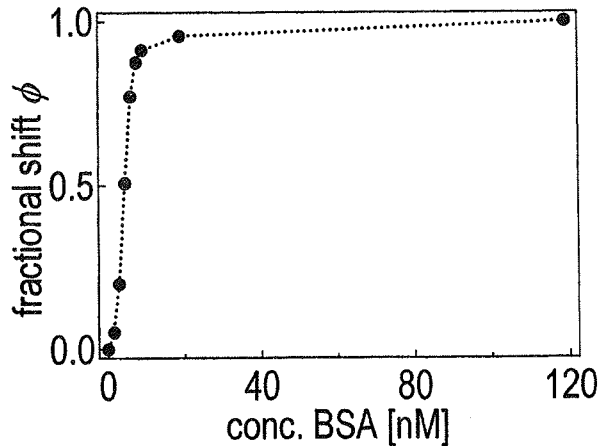


Fig.8 BSA adsorption measurements. (a) shows the shift of the microsphere resonance in real time. (b) adsorption isotherm.

Turns out that the student had retrieved the solution from a cooler so that the overall solution got a bit cooler upon injection, and the microsphere shrunk by a few tenths of a nanometer. This was evidenced by the slight drop in temperature recorded by the thermocouple (lower plot in Fig. 8a). With a little time for equilibrium to be re-established the negative wavelength shift began to recover and the experiment recorded an overall positive shift in wavelength of 0.02 nm. The BSA had adsorbed. The lower plot shows an isotherm for the process. Basically different concentrations of BSA were injected. The threshold for seeing a change was unprecedentedly small for unlabelled

adsorption (<1 nM). Although the experiment in Fig.8a was carried out for a solution concentration of 2 μ M. Fig.8b clearly shows that the adsorption process saturated above ~20nM. The shape reflected here is called a Langmuir isotherm. Where it flattens there is 100% coverage. That does not mean there are no voids, however before dealing with this question we want to show the dependence of the saturation shift on the radius of the microsphere.

Our theoretical results for for the fractional shift in wavelength at saturation (Eqns. 17 and 19) show a distinct inverse size dependence on microsphere radius. Fig.9 displays the measured size dependence.

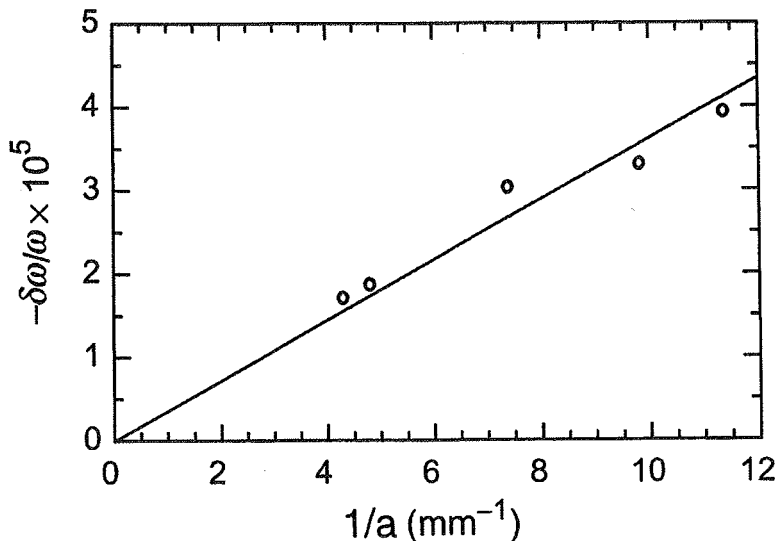


Fig.9 The dependence of the shift in resonance frequency on microsphere curvature.

The theory in this respect is clearly borne out. Furthermore, the slope of the plot (3.6 nm) can be compared directly with theory. From Eqn. 17 the slope is just the fractional shift times the microsphere radius, or more precisely

$$\text{Slope in Fig.9} = -a \frac{\delta\omega}{\omega} = \frac{(\epsilon_{rl} - \epsilon_{rm})}{(\epsilon_{rs} - \epsilon_{rm})} t. \quad (21)$$

If the permittivity of the layer were the same as that of silica, then the slope would be the thickness of the layer. In fact the permittivity of protein is known to be slightly larger than silica. So the thickness of the layer may be expected to be less than 3.6 nm. Since BSA is known from x-ray crystallography to be a thick heart shaped pancake with a dimension in the plane of ~6 nm and a thickness between 3, and 4 nm our measurement leads us to the conclusion that the largest area of the molecule is against the surface of the silica. This configuration should minimize the coulombic energy between the positively charged amine rug and the negatively charged protein. This

conclusion is in agreement with recent neutron reflection experiments which also show that BSA flattens to a 3 nm thickness due to the coulombic tug of the surface.¹⁴

Based on our existing data and the neutron reflection results we can take our analysis one further step. Since we expect voids to exist, and the wavelength is considerably larger than a molecule, we will express the permittivity of the layer in terms of a mean field approximation.

$$\epsilon_{r\ell} = f_p \epsilon_{rp} + (1 - f_p) \epsilon_{rm} . \quad (22)$$

where f_p is the fractional volume of protein in a layer of thickness t . Joining Eqn.22 with Eqn.21,

$$\text{Slope in Fig.9} = -a \frac{\delta\omega}{\omega} = \frac{f_p (\epsilon_{rp} - \epsilon_{rm})}{(\epsilon_{rs} - \epsilon_{rm})} t . \quad (23)$$

A protein molecule contains a polypeptide chain which includes 21 different amino acids. Because of this statistical mix of similar components, the refractive index from one protein molecule to the next is basically the same, $n_p \cong 1.50$.¹⁵ Water and silica have refractive indices which are well known and equal to 1.33 and 1.46, respectively. Using our measured slope (3.6 nm), a thickness of BSA from neutron reflectance (3.0 nm) along with the aforementioned refractive indices, f_p is found to be 0.90. This means that the void fraction is about 10%. Thus BSA forms an extremely compact monolayer. More compact than hexagonal close packed spheres in 2D.

Our results on BSA and on five other proteins agree with our perturbation model. This perturbation model enables us to extract slopes for variety of other proteins with molecular weights differing by orders of magnitude. We have discovered that the coulombic interactions between protein molecules and the amine groups drive the adsorption of molecules in a particular way, such that proteins deform in a similar aspect ratio (thickness divided by the square root of surface area occupied by protein) upon adsorption.¹⁶ It appears that the Photonic Atom adsorption sensor is an extremely sensitive realtime probe to nanoscopic layers. However, this lesson thus far has only scratched the surface.

The Photonic Atom sensor also acts as a biosensor. It can be used to identify the adsorbing molecule. It is important to note here that the means for doing this is not through conventional spectroscopy. Although chemists and physicists have traditionally learned to identify atoms and molecules by optical spectroscopy (absorption, fluorescents, etc.), there is not light deep in our cells. Yet our cells recognize tens of thousands of different proteins well enough to enable us to function. Much of this recognition is through shape complementarity aided by sticky physio-chemical interactions. For example in a sensitized person, the allergic reaction to certain toxic proteins on the surface of pollen grain, causes a specific antibody to engulf the invading allergen like a lock covering a key. This highly specific physio-chemical recognition will not occur with other proteins. Another example is the hybridization that occurs between complimentary strands of DNA. If we mimic biology, we would also sense biomolecules through dark interactions. The Photonic Atom Biosensor is

ideal for this purpose. Simply by attaching a biorecognition element to its surface, adsorption becomes specific. For example, antibody molecules can be attached for the detection of specific antibody-antigen interactions, or single stranded DNA for DNA detection through hybridization. This is not “pie in the sky”. The experiments have already been done with the Photonic Atom Biosensor.^{4,5}

There is much more to do. Perturbation theory will not simply stop at first order for the “light atom”, just as it did not stop at first order for the electronic atom. In addition there is a great deal to be done concerning single molecule detection.

Acknowledgements

Steve Arnold thanks Rino DiBartolo for his kind invitation to lecture at this school and for re-introducing him to the land of Rino's birth.

This was the second time Steve attempted to make a course out of his research. By learning from those who have done this in the past years, he gained a great deal of insight into the technique. Steve is particular indebted to Eric Mazur and Ralph von Baltz for their encouragement.

Without the prodding and encouragement from Ottavio Forte this manuscript would not have been completed on time. Bravo Ottavio.

Finally Mayumi Noto would like to thank the National Science Foundation for her fellowship and S. A. and M. N. would like to thank NASA for supporting work in thermal sensing using Photonic Atoms.

References

- 1 S. Arnold, Spontaneous Emission within a Photonic Atom: Radiative Decay Rates and Spectroscopy of Levitated Microspheres, in *Spectroscopy of Systems with Spatially Confined Structures*. Ed. by Baldassare DiBartolo (Kluwer Academic Publisher, 2002) pp.465-488
- 2 S. Arnold, M. Khoshshima, I. Teraoka, S. Holler, F. Vollmer, "Shift of whispering gallery modes in microspheres by protein adsorption," *Opt. Lett.* **28**, 272(2003).
- 3 I. Teraoka, S. Arnold, and F. Vollmer, "Perturbation approach to resonance shifts of whispering-gallery modes in a dielectric microsphere as a probe to the surrounding medium," *J. Opt.Soc.Am.B* **20**, 1937(2003).
- 4 F. Vollmer, D. Braun, and A. Libchaber, M. Khoshshima, I. Teraoka, and S. Arnold, "Protein detection by optical shift of a resonant microcavity," *Appl. Phys. Lett.*, **80**, 4057(2002).
- 5 F. Vollmer, S. Arnold, D. Braun, I. Teraoka, A. Libchaber, "DNA detection from the shift of whispering gallery modes in multiple microspheres," *Biophysical Journal* **85**, 1974(2003).
- 6 H.M. Nussenzveig, *Comments Atomic and Mol.Phys.* **23**, 175(1989).
- 7 J.C. Knight, G. Cheung, F. Jacques, and T.A. Birks, "Phase-matched excitation of whispering-gallery-mode resonances by a fiber taper," *Opt. Lett.* **22**, 1129(1997).
- 8 D.Q. Chowhury, S.C. Hill, and M.M. Mazumder, *IEEE J. Quantum Electron.* **29**, 2553(1993).
- 9 M. Khoshshima, *Perturbation of Whispering Gallery Modes in Microspheres by Protein Adsorption: Theory and Experiment*, PhD thesis, Polytechnic University, Jan. 2004.
- 10 L.M. Folan, "Characterization of the accretion of material by a microparticle using resonant ellipsometry", *Appl. Optics* **31**, 2066(1992).
- 11 J. D. Jackson, *Classical Electrodynamics*, Wiley, New York (1962), p. 753.
- 12 M-C Amann, J. Buus, *Tunable Laser Diodes* [Artech House Optoelectronics Library, (1998)]
- 13 D.C. Carter, X. M. He, S. H. Munson, P.D. Twigg, K. M. Gernet, M. B. Broom, and T.Y. Miller, "Three-dimensional structure of human serum albumin," *Science* **244**, 1195(1989).
- 14 T. J. Su, J. R. Lu, R. K. Thomas, and Z. F. Cui. "The effect of pH on the adsorption of bovine serum albumin at the silica/water interface studied by neutron reflection," *J. Phys. Chem. B.* **103**, 3727(1999).
- 15 P.A. Cupers, W. Th. Hermens, and H.C. Hernker, "Ellipsometry as a tool to study protein films at a liquid-solid interface", *Biochemistry* **84**, 56(1978).
- 16 M. Noto, M. Khoshshima, G. Guan, D. Keng, and S. Arnold, "Molecular mass sensitivity of a whispering gallery mode biosensor," submitted.

